Supplementary information for "Kimberlite magmatism induced by west-dipping subduction of the North American Plate"

Wenbo Zhang[1*], Stephen T. Johnston[1], and Claire A. Currie[2]

[1]*Earth and Atmospheric Sciences, University of Alberta, Edmonton, AB, Canada, T5G2E3*

[2]*Department of Physics, University of Alberta, Edmonton, AB, Canada, T6G2E1*

Methods

The purpose of our study is to determine the deflection and stress profiles in response to elastic plate flexure. The deflection profile mainly helps us define a reference point, based on which we can determine the lateral stress distribution. We use a semi-infinite beam model (Timoshenko and MacCullough, 1935; Watts, 2001), where the elastic strength can be characterized by the flexural rigidity (D):

$$D = \frac{E\,T_e^{\,3}}{12(1-\nu^2)} \quad (1)$$

where E is Young's modulus, T_e is the elastic thickness of the plate, and ν is Poisson's ratio. The strength can also be characterized in terms of the flexural parameter (α):

$$\alpha = \sqrt[4]{\frac{4\,D}{(\rho_m-\rho_{infill})\,g}} \quad (2)$$

where ρ_m is mantle density (~3300 kg/m^3), ρ_{infill} is density of material that infills basins on top of the plate, and g is gravity acceleration (9.81 m/s^2).

The deflection at the top of the beam, as a function of horizontal distance (x) is given by:

$$W(x) = \frac{2P_b*\lambda}{(\rho_m-\rho_{infill})g}\,e^{-\lambda x}\cos(\lambda x) = W_0\,e^{-\lambda x}\cos(\lambda x) \quad (3)$$

The stress distribution along the bottom of the beam is:

$$S(x) = -\frac{E\,2P_b\lambda^3 \boldsymbol{T_e}}{(1-\nu^2)(\rho_m-\rho_{infill})g} e^{-\lambda x}\sin(\lambda x) = S_0\, e^{-\lambda x}\sin(\lambda x) \quad (4)$$

In equations (3) and (4), the P_b is the loading force acting on the free-end of the semi-infinite beam, and λ is the inverse of the flexural parameter (α). We define W_0 and S_0 to encompass all the variables that do not depend on x, and thus they are constants that modulate the amplitude of the stress and deflection profiles. For the stress distribution along the base of the elastic beam (equation (4)), positive and negative values represent extension and compression, respectively.

Table S1 gives the parameters used for the continental and oceanic plates in our calculations. Young's modulus, which describes the ratio between uniaxial stress and strain, commonly ranges between 0 and 100 GPa for rocks (Watts, 2001; Turcotte and Schubert, 2002). In our experiments, we assume that the Young's modulus of continental lithosphere (e.g. craton with CCKC) is 70 GPa (Turcotte and Schubert, 2002). Oceanic plates (with 80 GPa), being more mafic than continental plates, tend to have a higher Young's modulus. Poisson's ratio describes the ratio between lateral and axial stresses (Johnson and DeGraff, 1988; Watts, 2001; Turcotte and Schubert, 2002). We use a Poisson's ratio to 0.3 which is a common value for the crust and rigid upper mantle (Catchings, 1999; Watts, 2001). The infill density depends on the material overlying the flexed plate. Here, we assume that the material on top of the cratonic lithosphere is continental sediments with a density of 2200 kg/m^3 (Turcotte and Schubert, 2002) and on top of the oceanic plate is water with a density of 1000 kg/m^3. We choose elastic thickness values based on studies of flexure for the Japan trench outer rise (Levitt and Sandwell, 1995; Turcotte and Schubert, 2002) and the Cordilleran foreland basin (Beaumont, 1981; Flück et al., 2003) (see discussion below).

For a bending elastic beam, equation (3) expresses the deflection in the horizontal direction. We choose the point with no deflection as our reference point, corresponding to a horizontal distance of $\alpha\pi/2$ from maximum deflection. This reference point is taken as the trench for a subducting slab. On the stress profile (equation (4)), we identify 3 key points at distance of: $\alpha\pi$, $5\alpha\pi/4$, $2\alpha\pi$. The region between $\alpha\pi$ and $2\alpha\pi$ is the area where tensile stresses are predicted at the base of the elastic beam. The point $5\alpha\pi/4$ is the location of maximum tensile stress.

Table S1. Parameters used in calculations

	Continents	Oceanic
Young's modulus (GPa)	70	80
Poisson's ratio	0.3	0.3
Elastic thickness (km)	120	60
Infill density (kg/m^3)	2200	1000
Mantle density (kg/m^3)	3300	3300
Flexural parameter (α, km)	250	130
Inverse of α (λ, km^{-1})	$3.95*10^{-9}$	$7.73*10^{-9}$
Flexural rigidity (D, Nm)	$1.11*10^{25}$	$3.75*10^{24}$

Normalization of stress and deflection plots

In Fig. 3, vertical axes for both stress and deflection are normalized and thus are dimensionless. In the normalization, all constants in equation (3) and (4) are equal to W_0 and S_0, respectively. Therefore, normalized values for deflection (W') and stress (S') are:

$$W' = \frac{W}{W_0} = e^{-\lambda x} \cos \lambda x \quad (5)$$

$$S' = \frac{S}{S_0} = e^{-\lambda x} \sin \lambda x \quad (6)$$

The reasons for normalization are that (1) P_b (the line load) is a term that is not constrained, and (2) W_0 and S_0 determine the magnitude of the plate deflection and stress but do not affect the wavelength. We are primarily interested in the lateral stress distribution in the direction of plate convergence (and thus orthogonal to the flexure axis) in our analysis as our goal is to relate this to the location of magmatism (Petit-spot volcanism and the CCKC).

Effect of variations in elastic parameters on the tensile stress distribution

In this section, we test the variations in the elastic parameters to investigate the effect on the location of tensile stresses in the lower part of the craton. We primarily focus on the elastic thickness because this factor plays the most important role in controlling the elastic strength, and thus resulting flexural profile, as it is cubed in equation (1). We vary the elastic thickness from 90 to 150 km, based on the range of values obtained from a study of gravity-topography coherence for the Canadian cratonic region (Flück et al., 2003). All other parameters are taken to be the continental values shown as in Table S1.

Fig. S1 shows that how resulting distribution of tensile stresses is affected by elastic thickness. With a greater elastic thickness, there is an increase in 1) the width of the tensile region and 2) the location of tensile stress relative to zero-deflection reference point. For the lowest elastic thickness (90 km), tensile stresses are found between ~240 and 710 km from the reference point (taken to be the trench), whereas for a 150-km elastic thickness, the tensile stress region is from ~470 to 1400 km relative to the reference point. The changes in the width and location of the tensile stress occur because a greater elastic thickness increases the flexural rigidity of the plate (equation (1)), resulting in a longer wavelength of the flexure.

Fig. S1 can also be used to assess the effects of other elastic parameters. If the elastic thickness is held at 120 km, variations in Young's modulus of ± 10 GPa from our preferred value of 70 GPa result in a flexural rigidity of 1.1 (± 0.15)*10^{25} Nm (equation (1)). Variations in Poisson's ratio of ± 0.1 (preferred value of 0.3) result in a flexural rigidity of 1.1 (± 0.1)*10^{25} Nm. These variations do not significantly affect the location or dimensions of the tensile stress region.

As shown in Fig. S1, the CCKC lies within the tensile stress region for all values of the cratonic elastic thicknesses from Flück et al. (2003). It should be noted that these are the modern-day elastic thickness values. Beaumont (1981) suggested that the flexural rigidity of North American craton in the Cretaceous was approximately 10^{25} Nm, based on the observed geometry of the Western Canadian Sedimentary Basin. This rigidity gives an elastic thickness similar to our preferred value of 120 km (Fig. S1).

Location of the CCKC

On Fig. S1, the location of the CCKC is shown as a 200-km wide band (red), with the black (median) line indicating the calculated CCKC location (700 km) relative to trench and ±100 km indicating the possible extent of the kimberlite. This band is consistent with the ~200-km wide kimberlite corridor shown on Fig. 1. The black line (Fig. S1) corresponds to the measured distance between the Omineca Magmatic Belt and the surface exposures of the kimberlite field near Saskatchewan (see main text), with a correction for Paleocene shortening, and under the assumption that the Omineca Magmatic Belt is assumed to be the volcanic arc located 300 km of the inferred trench (see main text). The arc-trench distance is based on the modern average, and this does exhibit variability (Syracuse et al., 2010). Therefore, there is

uncertainty in the arc-trench distance, as well as some uncertainty in the amount of shortening in the eastern Cordillera. The ±100 km band is taken to encompass these uncertainties, as well as account for the finite width of the kimberlite fields (5-10 km).

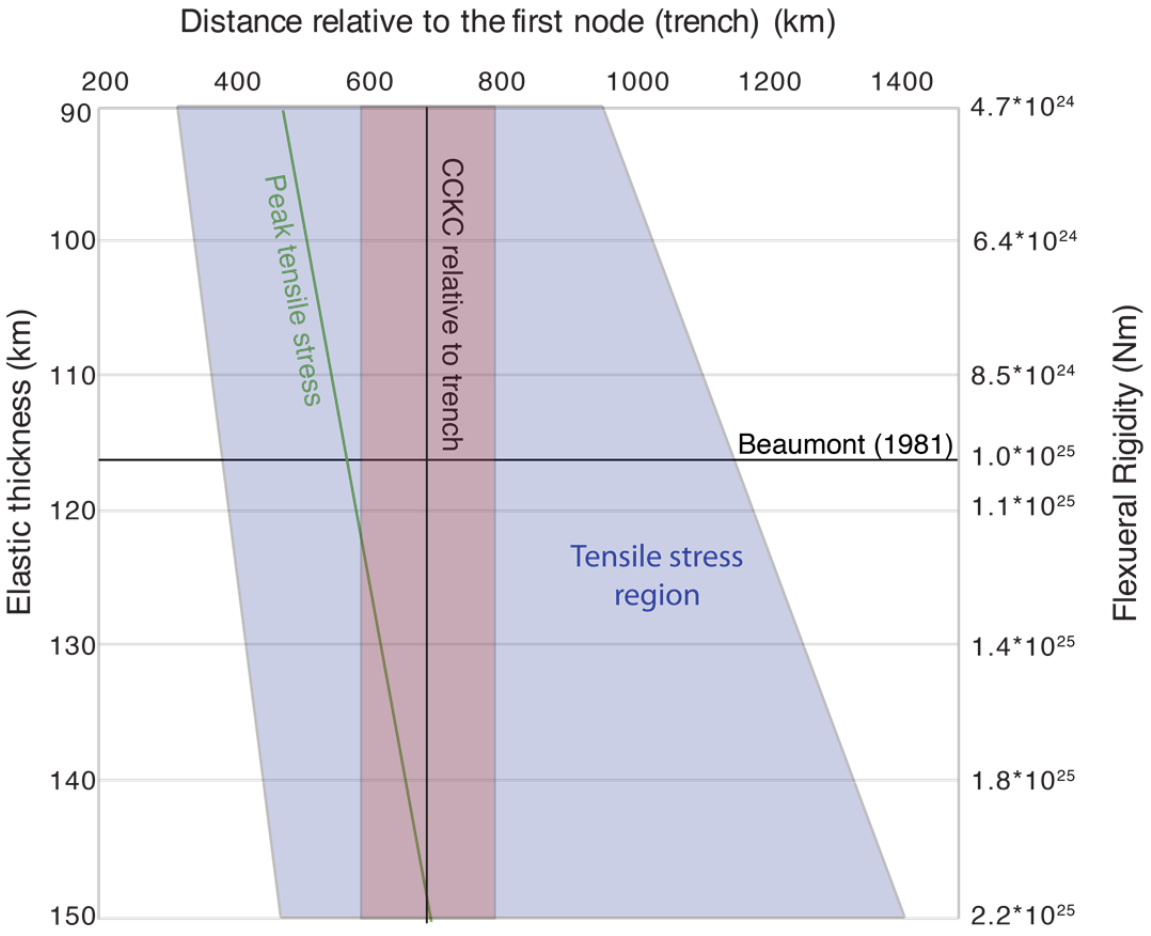

Figure S1. Effect of variations in elastic thickness and flexural rigidity on the distribution of tensile stress in the lower part of the craton. The purple region denotes where tensile stress occurs, with the green line showing the position of maximum tensile stress.

REFERENCES

Beaumont, C., 1981, Foreland basins: Geophysical Journal International, v. 65, p. 291–329, doi:10.1111/j.1365-246X.1981.tb02715.x.

Catchings, R.D., 1999, Regional Vp, Vs, VplVs, and Poisson's Ratios across Earthquake Source Zones from Memphis, Tennessee, to St. Louis, Missouri: Bulletin of Seismological Society of America, v. 89, p. 1591–1605.

Flück, P., Hyndman, R.D., and Lowe, C., 2003, Effective elastic thickness Te of the lithosphere in western Canada: Journal of Geophysical Research: Solid Earth, v. 108, doi:10.1029/2002JB002201.

Johnson, R.B., and DeGraff, J.V., 1988, Principle of Engineering Geology: Wiley, 512 p.

Levitt, D.A., and Sandwell, D.T., 1995, Lithospheric bending at subduction zones based on depth soundings and satellite gravity: Journal of Geophysical Research: Solid Earth, v. 100, p. 379–400, doi:10.1029/94JB02468.

Syracuse, E.M., van Keken, P.E., and Abers, G.A., 2010, The global range of subduction zone thermal models: Physics of the Earth and Planetary Interiors, v. 183, p. 73–90, doi: 10.1016/j.pepi.2010.02.004.

Timoshenko, S., and MacCullough, G.H., 1935, Elements of Strength of Materials: D. Van Nostrand Company, Inc.

Turcotte, D.L., and Schubert, G., 2002, Geodynamics: Cambridge University Press, 828 p.

Watts, A.B., 2001, Isostasy and flexure of the lithosphere: Cambridge; New York, Cambridge University Press, 105–110 p.